Broadband and Low-Random-Phase-Errors 2 × 2 Optical Switch on Thin-Film Lithium Niobate

Qiao Chen, Meng Ke Wang, Xiao Xia Ma, Hao Yao, and Kai Xin Chen, *Member, IEEE*

***Abstract*—We propose and demonstrate a broadband and low-random-phase-errors 2 × 2 optical switch on thin-film lithium niobate platform. The proposed switch is based on a typical Mach-Zehnder interferometer constructed with two 2 × 2 3-dB multi-mode interferometer couplers, two few-mode waveguide (FMW) arms, and corresponding input and output waveguides. The use of FMWs can help to reduce the random phase errors and improve the fabrication tolerances. Over a wide optical bandwidth from 1530 nm to 1605 nm, our typical fabricated switch can work on the desired initial operating state and achieve an extinction ratio mostly larger than ∼16 dB. The switching voltage is ∼7.3 V. The rise and fall times are 134.4 ns and 8.8 ns, respectively. This work can facilitate the development of optical switches on the lithium-niobate-insulator (LNOI) platform.**

***Index Terms*—Optical switch, electro-optic effect, optical waveguide, thin-film lithium niobite.**

I. Introduction

OPTICAL switches play an important role in optical communication and information processing systems, including data centers [1], quantum computing [2] and sensing [3]. To satisfy the ever-increasing demand for compact footprint, low power consumption, and high-speed switching, various kinds of optical switches have been proposed [4], [5], [6], [7], [8], [9]. These switches can be mainly divided into electro-optic (EO) switch and thermo-optic (TO) switch according to their operation principles. TO switches based on TO effect can usually realize small footprint with short phase shifters due to large thermo-optic coefficient of the used materials [8], [9], [10], [11], [12], [13]. But relatively large power consumption and long switching time of TO switches have always been an issue need to be addressed. In comparison with TO switches, EO switches are usually able to achieve a much faster switching speed. Therefore, EO switches based on different material platforms have always attracted extensive attention. Although the silicon-based EO switches using the free-carrier dispersion effect have been demonstrated, the free-carrier dispersion effect introduces large optical absorption loss [14], [15], [16]. While the polymer EO switches are simple to be fabricated, they are limited by temperature stability of polymers [17], [18].

For decades, lithium niobate (LN) has been attracted extensive attention due to its excellent properties, including large electro-optic coefficient, low optical loss, wide transparency window, good temperature stability and so on [19]. However, conventional LN EO switches have large device size due to the small index contrast of the used waveguides formed with the annealed-proton-exchanged (APE) or the Ti in-diffusion processes, which do not meet the demand of miniaturization [20], [21]. Fortunately, this defect has now been addressed by the new emerging thin-film lithium niobite, i.e., lithium niobate on insulate (LNOI). The LNOI platform can not only retain the excellent material characteristics of LN, but also enable high-index-contrast LN waveguide and, hence, compact LN waveguide devices, such as switch [7], tunable ring resonator [22], mode (de)multiplexer [23] and modulator [24]. Note that the EO switch in [7] is structured with hybrid integration of silicon and LNOI waveguides, which make its fabrication more complicated.

Mach-Zehnder interferometer (MZI) is widely used to structure high-performance optical switch with wide optical bandwidth, high extinction ratio (ER), and low driving power (TO switch) or voltage (EO switch). However, the random phase errors are easy to be introduced in waveguide arms of MZI optical switches due to the random variation in waveguide width caused by unavoidable fabrication errors [15], [25], [26], [27], [28]. Compared with using extra tuning mechanism to compensate the fabrication errors, which requires additional components and feedback control schemes with more power consumption [15], [25], [26], the passive solution by widening the waveguide arms is simpler and more attractive [27], [28].

In this letter, we propose a broadband and low-random-phase-errors MZI optical switch based on LNOI platform. Compared with the MZI switch in [7] structured with hybrid integration of silicon and LNOI waveguides, our proposed MZI switch is structured only with LNOI waveguide, which make it easier to fabricate. In our design, two identical few-mode waveguides (FMWs) are employed as the waveguide arms of the MZI switch. Thanks to the use of FMWs, which helps to reduce the random phase errors introduced in the fabrication process and improve the fabrication tolerances [29], our typical fabricated switch can work on desired initial state. And with a switching voltage of ∼7.3 V, the switch achieves an extinction ratio mostly larger

Manuscript received 2 November 2022; revised 30 November 2022; accepted 7 December 2022. Date of publication 12 December 2022; date of current version 22 December 2022. This work was supported in part by the National Natural Science Foundation of China under Grants 62075027 and U20A20165, in part by the Key Research and Development Program of Sichuan Province under Grant 2020YFSY0003, in part by the Key Technology R&D Program of Shenzhen under Grant JSGG20210802154413040, and in part by the Fundamental Research Funds for the Central Universities under Grants ZYGX2019J050 and ZYGX2020ZB015. *(Corresponding author: Kai Xin Chen.)*

The authors are with the School of Optoelectronic Science and Engineering, University of Electronic Science and Technology of China, Chengdu 611731, China (e-mail: chenqiao2050@163.com; wmk@std.uestc.edu.cn; maxiaoxia_cd@163.com; yaohao@std.uestc.edu.cn; chenkx@uestc.edu.cn).

Digital Object Identifier 10.1109/JPHOT.2022.3228264

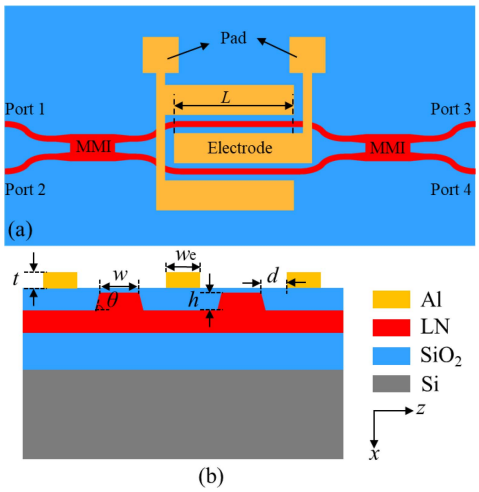

Fig. 1. Schematic diagrams showing (a) the top view of the proposed MZI switch and (b) the cross-sectional view of the two arms of the MZI switch.

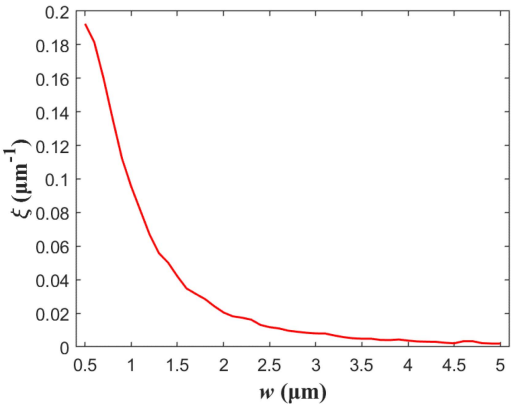

Fig. 2. Dependence of ξ with w at 1550 nm wavelength.

than ~16 dB and a crosstalk mostly less than ~−16 dB for each channel over a wide optical bandwidth from 1530 nm to 1605 nm. The rise and fall times are 134.4 ns and 8.8 ns, respectively.

II. Device Design and Fabrication

Our proposed 2 × 2 optical switch is shown schematically in Fig. 1(a), which is formed on an X-cut LNOI wafer. The structure of the switch is a typical MZI constructed with two identical FMW arms connected at the two ends with identical 3-dB 2 × 2 multimode interference (MMI) couplers. As shown in Fig. 1(b), the LN FMWs in the two arms have a top width of w, an etch depth (i.e., rib height) h, and a sidewall angle θ. To reduce the switching voltage, a set of push-pull electrodes using coplanar ground-signal-ground (GSG) configuration are used to drive the switch. Thus, the applied voltage can induce $\pm\pi/2$ phase shift in each arm due to the opposite direction of electric field across the two LNOI waveguides. The GSG electrodes with a length L, a thickness t, and a signal electrode width w_e, are placed symmetrically along the waveguides in the two arms with the same gap d to the waveguide arms, as shown in Fig. 1(a) and (b).

In our design, an X-cut LNOI wafer with a 600-nm-thick LN film and 5-mm-long aluminum (Al) GSG electrodes ($L = 5$ mm) are employed. The etch depth t and the sidewall angle θ of the waveguides are 300 nm and 70°, respectively. Additionally, all waveguides are placed along y direction so as to exploit the largest EO coefficient (r_{33}) of LN crystal. With above layout configuration, the switch can only achieve optimal operation for the transverse-electrode (TE) mode, and the parameters of the switch are chosen for this purpose.

Because of the inevitable random width variation introduced in the fabrication process, the random phase errors between the two arms of MZI are nonnegligible. Such an unexpected phase errors usually leads to that the fabricated optical switch does not operate at the optimal initial state (OFF state), i.e., the crosstalk is large when the switch is at OFF state. The large crosstalk at OFF state can be reduced effectively by widening the arm waveguides of the MZI appropriately, i.e., using FMWs as waveguide arms of the MZI. The random phase error $\Delta\varphi$ between the two arms of a MZI is defined as [27]

$$\Delta\varphi = \frac{2\pi}{\lambda_0}\,\xi\overline{\Delta w}L_w \tag{1}$$

where λ_0 is the operation wavelength in vacuum, ξ the derivative of the effective refractive index with respect to the waveguide width, $\overline{\Delta w}$ the mean width difference between the two arms, and L_w the length of the waveguide arms. Further, to compare the random phase errors $\Delta\varphi$ caused by the random width variation $\overline{\Delta w}$ for the waveguides with different width, we introduce normalized random phase error $\Delta\varphi/\overline{\Delta w}$ as in [27]. From (1), for a fixed L_w, $\Delta\varphi/\overline{\Delta w}$ is determined by ξ, and the smaller ξ, the smaller the normalized random phase error $\Delta\varphi/\overline{\Delta w}$. Fig. 2 shows the dependence of the derivative ξ with the width w of the waveguide arms at the wavelength of 1550 nm, calculated with a commercial mode solver (COMSOL). As the width w increases, ξ decreases rapidly at first and then slowly after $w > 2$ μm. Considering that a wider waveguide only slightly decreases the value of ξ and hence $\Delta\varphi/\overline{\Delta w}$, but results in a greater electrode spacing and therefore a larger switching voltage. Thus, to achieve an optimum trade-off between the normalized random phase error and the switching voltage, we choose $w = 2.5$ μm to design our proposed switch, which corresponds to a quite small $\xi = \sim 0.012$ μm^{-1} and $\Delta\varphi/\overline{\Delta w} = \sim 0.238$ rad/nm. As a comparison, we also design a reference switch with $w = 1.7$ μm, which corresponds to a somewhat larger $\xi = \sim 0.032$ μm^{-1} and $\Delta\varphi/\overline{\Delta w} = \sim 0.639$ rad/nm. These results indicate that, on the premise of achieving the same random phase error, a wider waveguide allows a larger $\overline{\Delta w}$, i.e., a larger fabrication tolerance than a narrower waveguide.

As a key component of our MZI switch, 2 × 2 MMI couplers are utilized, respectively, to split the input light signal into the two arms of the MZI and to combine the light signals from the two arms to achieve interference. To achieve a large ER and a low crosstalk, the 2 × 2 MMI coupler should realize power distribution in the two arms as equal as possible, i.e., an excellent 3-dB splitter. For our designed 3-dB 2 × 2 MMI coupler, its input/output waveguides are set at the edges of the multimode section according to the general interface mechanism [30]. In

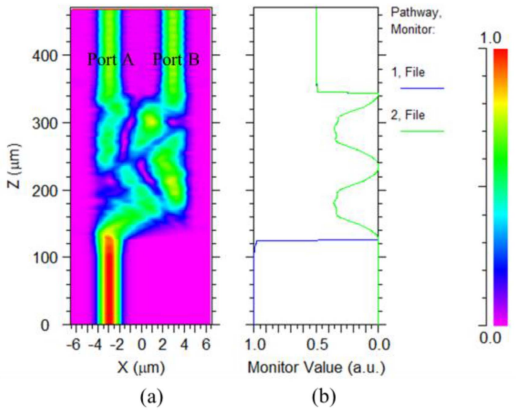

Fig. 3. Calculated (a) propagating light through the designed MMI coupler and (b) normalized power in the two output waveguides.

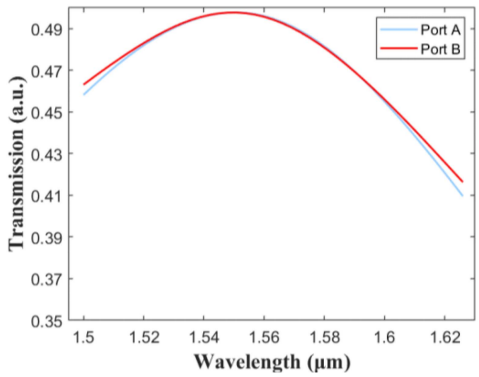

Fig. 4. Calculated transmission at the two output ports of the designed 2 × 2 MMI coupler at different operation wavelength from 1500 nm to 1620 nm.

our design, the multimode section has a width of 9 μm, while its length is calculated to be 219 μm with a three-dimensional finite difference beam propagation method (BeamPROP, RSoft). With above parameters, the calculated propagating light through the designed MMI and the normalized power in the two output waveguides are shown in Fig. 3(a) and (b). The power-splitting ratio is 40.1%:41.6% ∼ 50%:50% in the wavelength range from 1500 nm to 1620 nm for the fundamental quasi-TE mode, as shown in Fig. 4. To reduce the reflection and the mode mismatch loss at the junction [11], the linear taper waveguides with widths tapering slowly from 3.1 μm to 2.5 μm are introduced to connect the multimode section and input/output waveguides of the MMI couplers (see Fig. 1(a)). In addition, to minimize excitation of high-order modes, the S-bend waveguides with slow cosine profiles are used to connect the input/output waveguides and the MMI couplers as well as the MMI couplers and the FMW arms.

The proposed switch was fabricated with our in-house microfabrication facilities. A 150-nm-thick chromium (Cr) was first deposited on a commercial X-cut LNOI wafer with a 600-nm-thick thin film LN bonded on the 4.7-μm-thick buried oxide (BOX) layer. The designed MZI pattern was then defined on the Cr film by the standard ultraviolet (UV) photolithography and wet etching processes. Next, the MZI pattern was transferred into the LNOI by the proton-exchange process assisted by the dry etching method [31]. The measured etch depth was 298

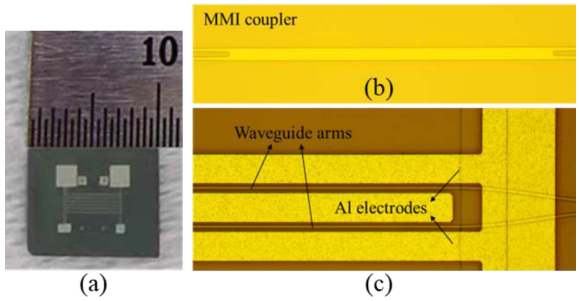

Fig. 5. (a) Photograph of the fabricated chip, (b) microscopic image of the MMI coupler, and (c) microscopic image of the waveguide arms and the electrodes.

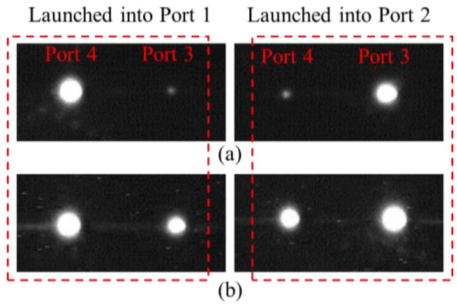

Fig. 6. Output near-field images from (a) the best one (S1) of the optimal switches with $w = 2.5$ μm and (b) one of the reference switches with $w = 1.7$ μm.

nm, which is very close to the design value (300 nm). After the residual Cr film was removed with a dechroming solution, a ∼400-nm-thick SiO_2 buffer layer was deposited on the chip to reduce the propagation loss and metal absorption loss. Subsequently, ∼600-nm-thick Al electrodes were formed on the SiO_2 layer by the thermal evaporation and lift-off processes. Finally, both input and output facets of the sample were polished carefully. Fig. 5(a) shows a photograph of the chip. There are three optimal switches of the same design of $w = 2.5$ μm and three reference switches of the same design of $w = 1.7$ μm. Fig. 5(b) and (c) are microscopic images of the MMI coupler, the waveguide arms, and the electrodes, respectively.

III. Experimental Results

We first characterized the output near-filed optical spot of the fabricated switches at the initial state to evaluate the random phase errors. Through a lensed single-mode fiber (SMF) with a polarization controller (PC) along the SMF, TE-polarized light at 1550 nm wavelength generated from a tunable laser was launched into Port 1 and 2 (see Fig. 1(a)) of the switch under test in turn. To avoid exciting any unexpected high-order modes in the device, the lensed SMF was aligned carefully with the input waveguide. We measured all six switches fabricated on the chip. In terms of the initial operating state, all three optimal switches are better than the three reference switches. The output near-field images from the best one (labeled S1) of the optimal switches and one of the reference switches, captured by an infrared camera (Micron Viewer 7290A), are shown in Fig. 6(a) and (b), respectively. Compared with the reference

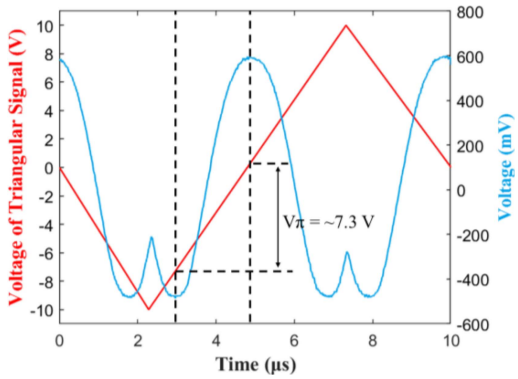

Fig. 7. Measured response signal with PD (blue) for the channel from Port 1 to 4 when a 100 kHz triangular electrical signal (red) was applied to the electrodes.

TABLE I
PERFORMANCE COMPARISON OF EO SWITCH ON LNOI PLATFORM

Extinction ratio (dB)	Switching speed Rise/Fall time (ns)	Switching voltage Cross/Bar state (V)	Optical bandwidth (nm)	Ref.
>26	0.1/0.312	8.59/3.62	1525-1570	7
>18.7	23/30	6.5	1530-1560	23
>16	134.4/8.8	7.3/0	1530-1605	This work

switch with $w = 1.7$ μm, this best switch with $w = 2.5$ μm is almost in the optimal initial state (i.e., the bar state), which indicates our proposed MZI switch achieves low random phase errors by widening the width of the waveguide arms.

To further evaluate the performance of S1, TE-polarized light at 1550 nm wavelength was launched into Port 1 and a 100-kHz triangular electrical signal from an arbitrary waveform generator (AWG) (Aim-TTi, TG5011A) was applied to the electrodes. The output light from Port 4 was detected with a photodetector (PD) (New Focus, Model 1811), analyzed with an oscilloscope (Tektronix, TDS 3054C), and shown in Fig. 7. From Fig. 7, the lowest point of the EO response signal (blue curve, see right vertical axis) corresponds to the ON state (cross state) of the switch, the corresponding driving voltage is ~ -7.3 V (red triangular electrical signal, see left vertical axis), while the highest point of the EO response signal corresponds to the OFF state (bar state) of the switch, the corresponding driving voltage is 0 V. Thus, the switching voltage i.e., the half-wave voltage (V_π) of our switch is $\sim$7.3 V, corresponding to a half-wave voltage-length product ($V_\pi \cdot L$) of 3.65 V·cm.

Further, we investigated the spectral response of S1 by launching the output light from an amplified spontaneous emission (ASE) source (B&A, AS4600, 1530-1605 nm) into Port 1 and 2 in turn with a lensed SMF. The polarization state of light was controlled with an inline fiber polarizer and a PC. The output light from Port 3/4 of S1 was collected with another lensed fiber and monitored with an optical spectrum analyzer (OSA) (Anristu, MS97740A). The measured transmission spectra when S1 operating at the ON (with a switching voltage of 7.3 V) and OFF states are normalized with respect to the spectrum of fiber to fiber and shown in Fig. 8(a) and (b), where the reference is the fiber-to-fiber transmission spectrum. It can be seen from

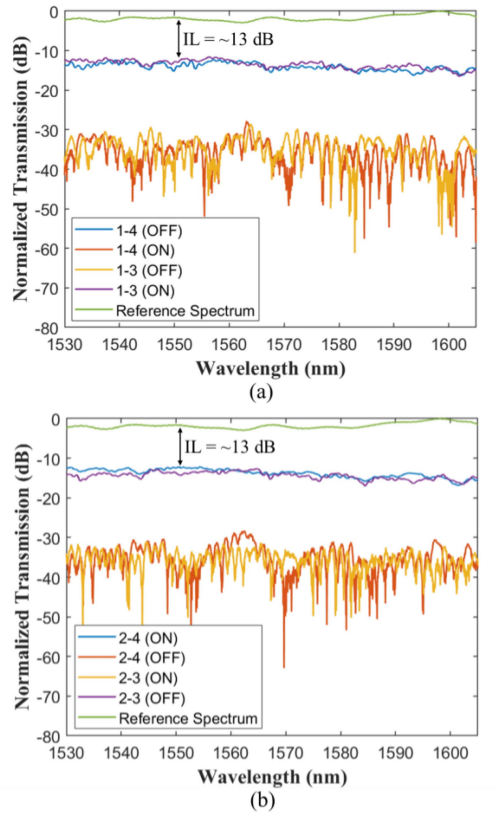

Fig. 8. Normalized transmission spectra (a) from Port 1 and (b) Port 2 to Port 3 and 4 when S1 operating at the ON and OFF states, where the reference is the fiber-to-fiber transmission spectrum.

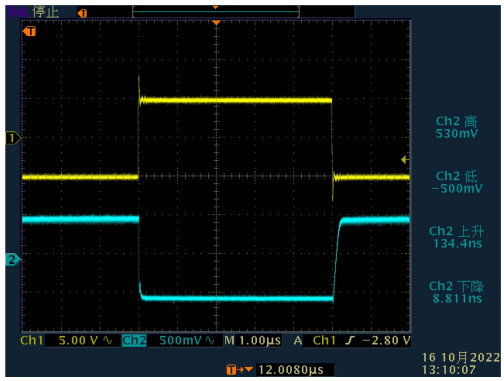

Fig. 9. Temporal switching characteristics of S1.

Fig. 8, the switch S1 exhibits almost the same ER and crosstalk characteristics for each channel over a wide range of wavelength from 1530 nm to 1605 nm. The ER is mostly larger than $\sim$16 dB, while the crosstalk is mostly less than ~ -16 dB. The wavelength range was limited by the light source available. The actual optical bandwidth of S1 should be much wider than the (C+L)-band shown in Fig. 8. In addition, the insertion losses of S1 for each channel are almost the same of $\sim$13 dB through comparing the reference spectrum with the transmission spectra of S1 shown in Fig. 8. Here, large insertion loss is mainly contributed by the large fiber-waveguide butt-coupling losses at the two ends because our devices do not incorporate edge couplers. It

should be possible to significantly reduce the insertion losses by integrating edge couplers on the switch [32], [33], [34], [35]. Although the fabrication of these edge couplers featuring bilayer [32], [33], [34] or step [35] structure is somewhat difficult, they actually help to achieve low fiber-waveguide butt-coupling loss of < 2 dB/facet, and a lowest loss of 0.5 dB/facet [34].

Finally, to evaluate temporal switching characteristics of S1, a 100-kHz square-wave signal with a duty cycle of 50% was applied to the electrodes. The measured temporal switching characteristics are shown in Fig. 9, which show that the fall and the rise time are 8.8 ns and 134.4 ns, respectively. For comparison, the performances of the EO switches on LNOI platform are summarized Table I. Compared with the mode switch in [23], our switch achieves comparable performance. While compared with the optical switch in [7], our switch has a smaller extinction ratio and a longer switching time but a lower switching voltage. And especially, our switch can achieve the bar state with a switching voltage of 0 V.

V. Conclusion

We have demonstrated a broadband and low-random-phase-errors 2×2 EO MZI optical switch on LNOI platform. We reduce the low random phase errors and improve the fabrication tolerances by using FMWs as the waveguide arms. Thanks to these efforts, our typical fabricated switch can work on desired initial state. And over a wide wavelength range from 1530 nm to 1605 nm, the switch achieves an ER mostly larger than $\sim$16 dB and a crosstalk mostly less than ~ -16 dB for each channel. The switching voltage is $\sim$7.3 V. The rise and fall times are 134.4 ns and 8.8 ns, respectively. This work can facilitate the development of optical switches on the LNOI platform.

References

[1] Q. Cheng, S. Rumley, M. Bahadori, and K. Bergman, "Photonic switching in high performance datacenters," *Opt. Exp.*, vol. 26, no. 12, pp. 16022–16043, 2018.

[2] A. Martin et al., "Photonic integrated circuit-based FMCW coherent LiDAR," *IEEE J. Lightw. Technol.*, vol. 36, no. 19, pp. 4640–4645, Oct. 2018.

[3] N. H. Wan et al., "Large-scale integration of artificial atoms in hybrid photonic circuits," *Nature*, vol. 583, pp. 226–231, 2020.

[4] X. Tu, C. L. Song, T. Y. Huang, Z. M. Chen, and H. Y. F, "State of the art and perspectives on silicon photonic switches," *Micromachines*, vol. 10, no. 1, Jan. 2019, Art. no. 51.

[5] R. Soref, "Tutorial: Integrated-photonic switching structures," *APL Photon.*, vol. 3, no. 2, Feb. 2018, Art. no. 021101.

[6] M. Thomaschewski, V. A. Zenin, C. Wolff, and S. I. Bozhevolnyi, "Plasmonic monolithic lithium niobate directional coupler switches," *Nat. Commun.*, vol. 11, no. 1, Feb. 2020, Art. no. 748.

[7] S. Q. Gao et al., "Fast polarization-insensitive optical switch based on hybrid silicon and lithium niobate platform," *IEEE Photon. J.*, vol. 31, no. 22, pp. 1838–1841, Nov. 2019.

[8] Q. Q. Song, K. X. Chen, and Z. F. Hu, "Low-power broadband thermo-optic switch with weak polarization dependence using a segmented graphene heater," *IEEE J. Lightw. Technol.*, vol. 38, no. 6, pp. 1358–1364, Mar. 2020.

[9] T. Kita and M. Mendez-Astudillo, "Ultrafast silicon MZI optical switch with periodic electrodes and integrated heat sink," *IEEE J. Lightw. Technol.,* vol. 39, no. 15, pp. 5054–5060, Aug. 2021.

[10] F. Duan, K. Chen, D. Chen, and Y. Yu, "Low-power and high-speed 2 × 2 thermo-optic MMI-MZI switch with suspended phase arms and heater-on-slab structure," *Opt. Lett.*, vol. 46, no. 2, pp. 234–237, Jan. 2021.

[11] S. P. Wang and D. X. Dai, "Polarization-insensitive 2×2 thermo-optic Mach–Zehnder switch on silicon," *Opt. Lett.*, vol. 43, no. 11, pp. 2531–2534, Jun. 2018.

[12] C. X. Wang et al., "Bottom-metal-printed thermo-optic waveguide switches based on low-loss fluorinated polycarbonate materials," *Opt. Exp.*, vol. 28, no. 14, pp. 20773–20784, Jul. 2020.

[13] X. B. Wang, W. Jin, Z. S. Chang, and K. S. Chiang, "Buried graphene electrode heater for a polymer waveguide thermo-optic device," *Opt. Lett.*, vol. 44, no. 6, pp. 1480–1483, Mar. 2019.

[14] M. R. Watts, W. A. Zortman, D. C. Trotter, R. W. Y oung, and A. L. Lentine, "Vertical junction silicon microdisk modulators and switches," *Opt. Exp.*, vol. 19, no. 22, pp. 21989–22003, Oct. 2011.

[15] J. V. Campenhout, W. M. J. Green, S. Assefa, and Y. A. Vlasov, "Low-power, 2 × 2 silicon electro-optic switch with 110-nm bandwidth for broadband reconfigurable optical networks," *Opt. Exp.*, vol. 17, no. 26, pp. 24020–24029, Dec. 2009.

[16] P. Dong et al., "Submilliwatt, ultrafast and broadband electro-optic silicon switches," *Opt. Exp.*, vol. 18, no. 24, pp. 25225–25231, Nov. 2010.

[17] W. Yuan et al., "Polymeric electro-optic digital optical switches with low switching voltage," *Electron. Lett.*, vol. 40, no. 3, pp. 195–197, Feb. 2004.

[18] Y. Enami, J. Luo, and K. Y. Jen, "Short hybrid polymer/sol-gel silica waveguide switches with high in-device electro-optic coefficient based on photostable chromophore," *AIP Adv.*, vol. 1, no. 14, Dec. 2011, Art. no. 042137.

[19] D. Zhu et al., "Integrated photonics on thin-film lithium niobate," *Adv. Opt. Photon.*, vol. 13, no. 2, pp. 242–352, Jun. 2021.

[20] H. L. Wang, X. P. Li, M. R. Zhang, and K. X. Chen, "Broadband 2×2 lithium niobate electro-optic switch based on a Mach–Zehnder interferometer with counter-tapered directional couplers," *Appl. Opt.*, vol. 56, no. 29, pp. 8164–8168, Oct. 2017.

[21] X. Y. Zhang et al., "An optical switch based on electro-optic mode deflection in lithium niobate waveguide," *IEEE Photon. Technol. Lett.*, vol. 32, no. 20, pp. 1295–1298, Oct. 2020.

[22] M. Zhang et al., "Broadband electro-optic frequency comb generation in a lithium niobate microring resonator," *Nature,* vol. 568, no. 7752, pp. 373–377, Apr. 2019.

[23] M. R. Zhang, K. X. Chen, M. K. Wang, J. Y. Wu, and K. S. Chiang, "Electro-optic reconfigurable two-mode (de)multiplexer on thin-film lithium niobate," *Opt. Lett.*, vol. 46, no. 5, pp. 1001–1004, Mar. 2021.

[24] C. Wang et al., "Integrated lithium niobate electro-optic modulators operating at CMOS-compatible voltages," *Nature*, vol. 562, no. 7725, pp. 101–104, Oct. 2018.

[25] S. K. Selvaraja, W. Bogaerts, P. Dumon, D. V. Thourhout, and R. Baets, "Subnanometer linewidth uniformity in silicon nanophotonic waveguide devices using CMOS fabrication technology," *IEEE J. Sel. Top. Quantum Electron.*, vol. 11, no. 6, pp. 316–324, Jan./Feb. 2010.

[26] C. M. Wilkes et al., "60 dB high-extinction auto-configured Mach-Zehnder interferometer," *Opt. Lett.*, vol. 41, no. 22, pp. 5318–5321, Nov. 2016.

[27] L. J. Song, H. Li, and D. X. Dai, "Mach-Zehnder silicon-photonic switch with low random phase errors," *Opt. Lett.*, vol. 46, no. 1, pp. 78–81, Jan. 2021.

[28] L. J. Song et al., "Toward calibration-free Mach-Zehnder switches for next-generation silicon photonics," *Photon. Res.*, vol. 10, no. 3, pp. 793–801, Mar. 2022.

[29] W. K. Wang et al., "Thin-film lithium-niobate modulator with a combined passive bias and thermo-optic bias," *Opt. Exp.*, vol. 20, no. 22, pp. 39706–39715, Oct. 2022.

[30] L. B. Soldano and E. C. M. Pennings, "Optical multi-mode interference devices based on self-imaging: Principles and applications," *J. Lightw. Technol.*, vol. 13, no. 4, pp. 615–627, Apr. 1995.

[31] X. P. Li, K. X. Chen, and Z. F. Hu, "Low-loss bent channel waveguides in lithium niobate thin film by proton exchange and dry etching," *Opt. Mater. Exp.*, vol. 8, no. 5, pp. 1322–1327, May. 2018.

[32] L. Y. He, M. Zhang, A. S. Ansari, R. R. Zhu, C. Wang, and L. Marko, "Low-loss fiber-to-chip interface for lithium niobate photonic integrated circuits," *Opt. Lett.*, vol. 44, no. 9, pp. 2314–2317, May. 2019.

[33] C. R. Hu et al., "High-efficient coupler for thin-film lithium niobate waveguide devices," *Opt. Exp.*, vol. 29, no. 4, pp. 5397–5406, Feb. 2021.

[34] P. Ying et al., "Low-loss edge-coupling thin-film lithium niobate modulator with an efficient phase shifter," *Opt. Lett.*, vol. 46, no. 6, pp. 1478–1481, Mar. 2021.

[35] M. K. Wang, J. H. Li, H. Yao, Y. J. Long, F. Zhang, and K. X. Chen, "A cost-effective edge coupler with high polarization selectivity for thin film lithium niobate modulators," *IEEE J. Lightw. Technol.*, vol. 40, no. 4, pp. 1105–1111, Feb. 2022.